Nanomanipulation: Buckling, Transport and Rolling at the Nanoscale

Richard Superfine
rsuper@physics.unc.edu
(919) 962-1185
Department of Physics and Astronomy,
Curriculum in Applied and Materials Sciences
Phillips Hall CB3255
University of North Carolina
Chapel Hill, NC 27599

Michael Falvo
falvo@physics.unc.edu
(919) 962-9346
Department of Physics and Astronomy,
Curriculum in Applied and Materials Sciences
Phillips Hall CB3255
University of North Carolina
Chapel Hill, NC 27599

Russell M. Taylor II
taylorr@cs.unc.edu
(919) 962-1701; FAX: (919) 962-1799
Department of Computer Science, Physics and Astronomy and the Curriculum in Applied and Materials Sciences
Sitterson Hall, CB3175
University of North Carolina
Chapel Hill, NC 27599-3175

Sean Washburn
sean@physics.unc.edu
(919) 962-9382
Department of Physics and Astronomy,
Curriculum in Applied and Materials Sciences
Phillips Hall CB3255
University of North Carolina
Chapel Hill, NC 27599

Report Documentation Page

Form Approved
OMB No. 0704-0188

1. REPORT DATE	2. REPORT TYPE	3. DATES COVERED
2002		**00-00-2002 to 00-00-2002**

4. TITLE AND SUBTITLE	5a. CONTRACT NUMBER
Nanomanipulation: Buckling, Transport and Rolling at the Nanoscale	5b. GRANT NUMBER
	5c. PROGRAM ELEMENT NUMBER
6. AUTHOR(S)	5d. PROJECT NUMBER
	5e. TASK NUMBER
	5f. WORK UNIT NUMBER
7. PERFORMING ORGANIZATION NAME(S) AND ADDRESS(ES) **Rice University,Department of Physics and Astronomy,Houston,TX,77005**	8. PERFORMING ORGANIZATION REPORT NUMBER
9. SPONSORING/MONITORING AGENCY NAME(S) AND ADDRESS(ES)	10. SPONSOR/MONITOR'S ACRONYM(S)
	11. SPONSOR/MONITOR'S REPORT NUMBER(S)

12. DISTRIBUTION/AVAILABILITY STATEMENT
Approved for public release; distribution unlimited

13. SUPPLEMENTARY NOTES

14. ABSTRACT

15. SUBJECT TERMS

16. SECURITY CLASSIFICATION OF:			17. LIMITATION OF ABSTRACT	18. NUMBER OF PAGES	19a. NAME OF RESPONSIBLE PERSON
a. REPORT **unclassified**	b. ABSTRACT **unclassified**	c. THIS PAGE **unclassified**		**51**	

NANOMANIPULATION: BUCKLING, TRANSPORT AND ROLLING AT THE NANOSCALE

1. INTRODUCTION

The study of novel materials produces many challenges in the areas of synthesis, modeling and characterization. For the latter, one would like to be able to determine mechanical, electrical and dynamical properties, and correlate them with structure. Correspondingly, a new perspective is emerging in biology where the significance of studying individual proteins and macromolecular structures is being appreciated to understand the details of molecular binding, transport and kinetic pathways. Enabling this revolution in nanoscale science has been the development of microscopy techniques that measure structure and many material properties. The atomic force microscope (AFM) provides a wide range of characterization capabilities (electrical, mechanical, chemical, etc.) on the nanometer scale, while correlating these with structure in the form of detailed topography.[1] Impressive as these capabilities are, the AFM can also be used as a nanometer-scale manipulation tool. The ability to manipulate objects efficiently on surfaces makes available a wide variety of experiments on the interactions between the sample and substrate,[2-4] on the physical properties of individual objects and on the creation of unusual devices incorporating the nanometer objects.[5,6]

In the laboratory the scientist must use an instrument to probe the nanoscale world. The challenge for the instrument developer is to enable ever-increasing resolution of material structure and properties. The advances in instrumentation are often characterized as ever increasing spatial resolution, smaller force detection, smaller electronic current measurement. Beyond these obvious considerations, two other challenges emerge as equally important: the interface between the scientist and the

instrument, and the combination of characterization techniques.[7] The ultimate goal of an interface is to make the instrument transparent for the scientist. Actions to be performed within the nanoscale world should feel as natural as performing them on a table-top object. Also, the visualization of data should be as natural as looking at the object under study as if it is being held in hand. As we continue to probe molecular systems, we need to correlate a wide range of physical and chemical properties with structure, all at the same time. This necessitates the ability to measure mechanical, electrical, dynamical and structural properties all within the same instrument.

In the following chapter, we describe work performed at the University of North Carolina-Chapel Hill (UNC) in the development of microscopy instrument systems, including a natural interface for scanned probe microscopy we call the nanoManipulator. We describe the principle design features of the instrument system including the visual display of data, the haptic (force-feedback) control and display capabilities. Second, we describe the combination of microscopy and manipulation in a joint Scanning Electron Microscopy/Scanning Probe Microscopy system. These systems have been used for studies of nanotube mechanical dynamical and electrical properties,[8] and for the study of biological macromolecular structures such as viruses, fibers (pili, fibrin, microtubules, etc.) and molecules (DNA).[9] We describe examples of these studies drawn from our work on nanotubes and viruses.

2. INSTRUMENTATION SYSTEMS: THE NANOMANIPULATOR AND COMBINED MICROSCOPY TOOLS

2.1 THE NANOMANIPULATOR: THE SCIENTIST AS AN ACTOR IN NANOSCALE SCIENCE

The goal of our interface development has been to allow the scientist to be an actor in the nanoscale world. We have combined microscopy with a virtual reality interface to provide the intuitive display of instrument data and natural control of the instrument functions. The significance of the virtual-reality interface to the SPM is that it gives the scientist simulated *presence* on the sample surface. The benefits of this are: improved perception of 3D structures, more effective exploration of the sample, the ability to observe dynamic processes in near real time, and the ability to interactively modify the surface. To put it in plain language: when you are present somewhere, you can look around, you can look at things from different angles, you can feel interesting things at arm's length, you can watch the behavior of things that move or change, you can pick up things and rearrange them, and you can tweak things to see how they respond. The ideal human interface for a scanning probe microscope (SPM) might present its user with a scaled-up 3D representation of the surface that can be probed and modified with a physical hand-held tool. The control system would translate tool motion into motion of the SPM tip and translate measured surface parameters into force pushing back on the tool, as well as visual and auditory representations of surface data. When using such a system, a scientist would seem to be interacting directly with the surface itself. Natural motions of head and hand would be used to investigate and sculpt the surface as if it were physically present at the scale of the scientist. This would allow the scientist to concentrate fully on investigating the surface and its features, rather than on programming the interface. A complete description of virtual reality interfaces for

microscopy is available elsewhere.[7] Here we provide here a brief description of the representative features of this system, including the display of information through visualization and haptics and the control of the instrument. The nanoManipulator, as diagrammed in Figure 1, consists of a scanning probe microscope with its controller, a PHANToM force-feedback device with its controller and a PC computer with graphics card. These three computers communicate across an IP-based network.

2.1.1 Display of data: visualization and haptics

The SPM is a highly refined instrument for exploration and manipulation at the nanometer scale. Many experiments have been done using preprogrammed or open-loop control of the SPM tip and feedback parameters during modification, and using pseudo-color or line-drawn images to display the collected data.[10] In a later section we describe the various modes of control of the microscope. Here we focus on the display of data. In addition to surface topography data, SPMs can also acquire many other data sets. These include conductance and current/distance measures (scanning tunneling microscopy), lateral force and adhesion (AFM), laser transmission at various wavelengths and polarizations (near field optical microscopy), magnetic properties (magnetic force microscopy), temperature and other parameters.[11] Few if any of these have natural mappings to visual channels such as color or height, but nonetheless the scientist may want to view the correlations between these data sets and topography. In these cases, it is useful to display the parameter visually in a non-realistic but still useful manner. For scientific visualization, the usefulness of a technique is more important than its realism. We have studied and developed many approaches for the visualization of single and

multiple data sets.[12,13] Here we review the simple issue of the 3D rendering of a surface, as an example of the considerations involved.

In the simplest case, the sample data is the surface topography. This is most naturally displayed as a 3d data set: a directionally illuminated surface. Using off-the-shelf PC's, it is now possible to have real-time rendering of surfaces as the data is acquired from the microscope. We provide real time interaction with viewing parameters such as illumination direction, viewing angle, and scaling through the force feedback pen. The 3D view is not always better: for flat surfaces with small features, a pseudo-color view is superior to the shaded 3D view. This is true for two reasons: the pseudo-coloring devotes the entire intensity range to depth and it also obscures small fluctuations caused by noise in the sampled image. For features that are significant only for their height difference from the rest of the image, the pseudo-color image devotes its entire range of intensities to showing this difference. This is equivalent to drawing the surface from above using only ambient lighting with intensity based on height. Any 3D shading of the image uses some of this range to accommodate the diffuse and specular components at the expense of the ambient component. This shift from ambient to diffuse/specular is a shift from displaying height to displaying slope (since angle is what determines the brightness of the diffuse and specular components). This works well for a noise-free image, but real-world images contain noise. For SPM images, a flat surface has the highest percentage of noise as a fraction of feature size. The noise causes fluctuations in illumination of the same magnitude as those caused by features, sometimes completely obscuring them. However, small features on surfaces with other height variations are

better brought out using specular highlighting of a 3D surface (and are often imperceptible in a 2D display).[7]

Furthermore, the scientist's ability to recognize specific molecular structures within the noisy, sampled data is improved by using stereoscopic, shaded 3D color graphics with specular highlights. Providing stereoscopic, rather than monoscopic, viewing is useful to the scientist because the stereo provides a direct perception of depth for nearby virtual objects. Allowing accurate perception of the 3D spatial structure of STM data makes it possible for scientists to use their own specialized knowledge to recognize structures and features of interest in the data.

It is intriguing to think of giving the scientist the ability not only to see the surface under the SPM, but actually to reach out and touch it. Conceptually, this is equivalent to a telerobotic system that operates across a great difference in scale, rather than over a great distance. We employ a force feedback pen that senses the 3d position of the pen tip (with additional capability to sense a total of 6 degrees of freedom) while also applying force to the user’s hand. The position of the pen in space can control various visualization features such as virtual “grabbing” of the surface to change viewing angle. However, it is during modification that force feedback has proved itself most useful by providing intuitive control of the probe tip position and sensing of the surface contours. This ability allows finer control and enabling whole new types of experiments. Force feedback has proved essential to finding the right spot to start a modification, finding the path along which to modify, and providing a finer touch than permitted by the standard scan-modify-scan experiment cycle. Force feedback allows the user to locate objects and features on the surface by feel while the tip is being held still near the starting point for modification.

Surface features marking a desired region can be located without relying only on visual feedback from the previous scan. This allowed a collaborator to position the tip directly over an adenovirus particle, then increase the force to cause the particle to dimple directly in the center. It also allowed the tip to be placed between two touching carbon filaments in order to tease them apart.

Finally, the nanoManipulator system records all data taken, including topography and external channels such as conductance, as a time sequenced data set we call a streamfile. This file can be replayed at a later time to review the entire experiment, including the complete correlation of property measurements with updating images of the sample structure. The user is not left with a record of the data as determined by decisions made at the time of the experiment. Often the important data is not appreciated until after the experiment is over. This has been widely appreciated in our group, where many of our most exciting insights have been discovered in post-experiment reviews of streamfiles.

2.1.2 Instrument control: haptics, virtual tips and on-the-fly mode switching

A manipulation can be performed most intuitively by allowing the users natural hand motions to control the trajectory of the probe tip. We have implemented several strategies for this control. The simplest technique is to allow the computer to control the force applied by the tip on the sample through a feedback loop, while the user's hand motion controls the lateral position of the tip. When the user moves the hand held pen up and down, she feels a "virtual" surface, such that when the hand is above a designated reference plane, no force is felt. As she lowers her hand and the pen crosses this reference

plane, a force is displayed to her hand that reflects the local topography data. Complete control over the tip in 3 dimensions has been implemented whereby the up and down motion of the users hand controls the motion of the probe tip in the z direction, normal to the surface. To prevent the crashing of the tip into the surface, we have implemented a force limit that returns control of the tip to the computer if the user exceeds a designated applied force.[7]

During the course of a manipulation, it becomes clear that the straightforward approach of pushing the object with the AFM tip will not be the most efficient. In the control mode where the user determines the position of the tip through the handheld stylus, similar to how the computer moves the tip during a raster, the object is observed to move off to the side of the tip. The reasons for this are obvious, in a naïve sense, to anyone who has pushed a tennis ball with a screwdriver. In performing such an operation, a user is likely to reach for another pushing tool, such as a flat-bladed spatula, which would present a broader surface to the object. While fabrication techniques for tips are reaching a high art, it is clearly impractical to have on hand a range of tip shapes for the range of tasks that might have to be accomplished. We have addressed this issue through the implementation of what we call *virtual tips*, whereby the AFM tip is moved by computer control along a trajectory at speed much faster than the average translation of the tip. The tip then appears to have shape that can be controlled by the computer. Several of these shapes are described below, including sharp, blunt, sweep, comb and roll modes. In addition, for AFM-based machining of metal and polymer films, we have implemented sewing mode, whereby the tip is lifted and pressed into the surface in order to machine narrow lines.

1. Sharp Mode- no sub-trajectory.

2. Blunt Mode- tip moves in a triangular pattern with leading point of triangle oriented along the pen path. The size of the diamond can be varied.

3. Sweep Mode- tip moves back and forth along a line. The length and the orientation of the line with respect to the average path are dynamically controlled by the use of two of the angular degrees of freedom of the hand-held force device.

4. Sewing Mode- tip moves in the z-direction normal to the surface. It is alternately raised to a pullback position and pressed to a set-point force. This can be implemented as either a fixed-frequency oscillation or as a fixed step size between presses.

5. Comb Mode- this is a lateral “tapping” mode where the tip is moved along a line as in sweep mode, but takes excursions in the perpendicular direction at proscribed distances. This allows the tip to move across an extended object, such as a tubular virus, and nudge it along its length while always releasing in the local normal direction. In this way the tip does not rub along the object, avoiding possible damage from frictional forces.

The above techniques have been tested in a variety of circumstances. Sharp mode is currently used the most for feeling and for manipulation. Blunt mode has been used in some cases to reduce noise during feeling. Sweep mode is widely used for both manipulation and for lithography, especially the manipulation of stiff objects such as nanotubes where it allows for controlled translation without rotation. There are several other techniques that might play an important role in the manipulator’s toolbox. These modes are corral mode and roll mode. Corral mode has been implemented to address the

manipulation challenges of small clusters where the object is observed to role off to the side of the tip. A possible remedy is to have the tip move along a trajectory where the tip is hitting the object from a range of angles, with the mean direction determined by the trajectory of the stylus motion.[7]

An AFM typically operates in one of two modes, *contact mode* or *vibrating mode*. Contact mode is described in the introduction, where the tip scrapes along the surface. Vibrating mode oscillates the tip at its resonance frequency (around 100kHz) and pushes towards the surface until the amplitude of oscillation is reduced to a fraction of its value away from the surface. Vibrating mode does not scrape the surface as much as contact mode does, so it provides damage-free scanning on more surfaces. The nanoManipulator interface allows switching between contact and vibrating modes without retracting the tip. [14] This allows a wider range of interaction forces between imaging and modification. Unfortunately, the positioning elements in the microscope undergo a sharp jump during the transition from one mode to the other. This results in a transient offset where the surface height appears to jump and then to relax to its new height over several seconds. This is compensated for automatically by the nanoManipulator, avoiding what would otherwise be sharp force discontinuities as the user goes from feeling to modifying the surface.

2.2 COMBINED SCANNING ELECTRON/ SCANNING PROBE MICROSCOPY

Most recently, we have combined an AFM, a scanning electron microscope (SEM) and the nanoManipulator interface to produce a manipulation system with simultaneous electron microscopy imaging.[15] Manipulation in the AFM has the limitation

of not being able to view the full orientation of the manipulated object during the manipulation. This is because there is only a single tip, and it can either image or manipulate at one time. Only after the manipulation is completed is the tip returned to an imaging mode and the user can understand the results of the manipulation. Scanning Electron Microscopy has been used for a wide range of surface characterization and imaging applications. Unfortunately, the electron beam is incapable of maneuvering objects or measuring their mechanical interactions. With a combined system of the SEM and the AFM manipulations can be viewed in real time to view material deformations and to precisely place nanoscale objects with respect to each other, or within devices. In this way, more sophisticated nano-structures can be created, and measurements can be performed by placing nano-objects within other measuring devices.

There have been several advances made to the user interface to take advantage of these new capabilities. First, we have implemented full three dimensional control of the AFM tip with the haptic interface, as described above. When the user moves the handheld pen in three dimensions, the tip follows the corresponding trajectory within the SEM chamber. The force applied by the tip to the sample is conveyed to the user, and a force limit is imposed on the interface so that the user cannot arbitrarily crash the tip. Second, the new system presents challenges in combining two data sets from different imaging techniques, each with their own set of artifacts. These include instrument response functions, drift and skew of the image, to name a few. We are currently developing strategies for accounting for the limitations of the individual imaging techniques through image modeling, and performing a combining procedure that will provide a best-case reconstruction using the information from the two data sets.

3.1 NANOMANIPULATION FOR MECHANICAL PROPERTIES

The mechanical properties of nanoscale materials are of great interest due to the potential lack of defects. In macroscopic samples, mechanical properties can be limited by the presence of defects that can promote sliding of shear planes and fracture. In addition, nanoscale structures may have shapes that are not found in typical materials. An example of this is the nanotube with a hollow core, such as has been found in carbon and non-carbon varieties. In these materials, new modes of deformation may arise that enable the material to perform new functions as objects in device settings or in functional materials. Manipulation of nanoscale materials can offer the ability to apply large strains with the accompanying observation of the resulting deformation and its possible reversibility.

We have used the nanoManipulator interface for AFM to perform intricate bending of carbon multiwall nanotubes (CNT) to large strains. A carbon nanotube consists of a graphite sheet wrapped seamlessly onto itself to form a tube.[16] They exist in single wall form, SWCNT [17] and multiwall form, MWCNT,[18] where the tube wall is made of many concentric shells. The SWCNT often come in a “rope” or “bundled” form where many individual tubes are close-packed in parallel. CNTs are have been shown to exhibit extraordinary electrical and mechanical properties.[19] The tubular structure takes advantage of the high basal-plane elastic modulus of graphite to produce a fiber predicted to have mechanical properties that surpass those of any previously known material.[20,21] We have observed a variety of behaviors including bending with and without periodic buckling, as well as large bends that are accommodated either by dramatic, irreversible

structural changes or by smooth changes without apparent damage. In the first series of images, a CNT, pinned at one end by carbon debris, was bent into many configurations. Figure 2 shows a series of 29 images where the CNT was bent repeatedly back and forth upon itself. The nanotube is never observed to fracture, even with a strain as large as 16% as measured along its outside wall in the tightest bend.[22] Insight into the remarkable behavior of the nanotube is given through an analysis of another nanotube that had been carefully bent at small radii of curvatures.

The inset of Figure 3A shows this second tube in its original adsorbed position and orientation. The abrupt vertical step on the left side of the tube was used as a reference mark (s=0) for feature locations. This CNT was taken through a series of 20 distinct manipulations alternately bending and straightening the tube at various points. We present images from this sequence to highlight specific features. Along with AFM topographic data, we also present the tube height along the tube's center as determined by the cores method[23] along with the calculated curvature. We will refer to raised points on the tube as "buckles", consistent with the increase in height expected from the collapse of a shell in response to bending. We observe two behaviors in this sequence: small, regularly distributed buckles at regions of small curvature and large deformation at high curvatures.[22,24,25]

We focus first on the regularly spaced buckles occurring in the more gradually bent region (lower right). Figure 3B and 3C show the tube as it is bent in opposite directions. The location of the buckles has shifted dramatically, with the buckles of Figure 3C appearing in regions which had been featureless, and the buckles of Figure 3B largely disappearing. The buckles appear with a characteristic interval independent of

their absolute position along the tube. These findings suggest that the buckling is reversible, intrinsic to the CNT and not mediated by defects. The strong correlation between tube curvature and the location of buckles confirms their role in reducing curvature-induced strain. Buckling in bent shells are well known in continuum mechanics [26] where two modes of deformation result from pure bending stresses. The Brazier effect causes the circular cross section of the tube to become more "ovalized" uniformly over the whole tube length [27] as the bending curvature increases. Bifurcation, on the other hand, leads to a periodic, low amplitude rippling of the tube wall on the inside of the bend (the portion under compression).

These experiments showed the remarkable strength of the nanotube is accompanied by a resiliency that is promoted by its shape as a hollow cylinder. Upon bending, the nanotube can release the strain on its outer (tensile) and inner (compressive) surfaces by buckling. This indicates that in applications as fillers in composite materials, the nanotube may show elasticity to high strains in both tension and in bending due to the ability of the hollow core to collapse.

3.2 NANOSCALE DYNAMICS: ATOMS AS GEAR TEETH

The relative motion of objects in contact is a ubiquitous phenomenon, appearing in the lubricated contact of macroscopic objects and increasingly playing a role in nanometer-scale electromechanical structures.[28,29] Over the past decade, new experimental techniques such as the Surface Force Apparatus (SFA)[30] and Atomic Force Microscopy (AFM) have obtained an atomic-scale view of moving interfaces. Through such studies, the intrinsic dependence of friction on contact area [2,31] and the dependence

of friction on crytallographic orientation have been identified. AFM studies have performed friction mapping of surfaces with atomic resolution,[32] and the identification of stick-slip motion for nanometer-scale objects.[3] Nanomanipulation provides the opportunity to take an object with atomically smooth and clean surfaces and study its full range of motion in a variety of contexts. Here we describe our experiments with carbon nanotubes which provide a laboratory for atomic lattice ineteractions.

Friction at the nanoscale differs from macro or micro friction in the degree of order of the contact. As in the case of mechanical properties, in a macroscale or micron scale contact, the frictional properties can be dominated by defects, and represent an average over many crystalline orientations. In a nanometer scale contact, we have the possibility of having a single crystalline orientation dominate the interfacial dynamics. New behavior emerges due to relative perfection and smoothness of the contacting surfaces [2] and the *ability to tune precisely the relative orientation of contacting atomic lattices*.

In this case the atomic structure matters. The arrangement of the atoms in two interacting surfaces has been shown to play a critical role in the energy loss that occurs when one body slides over a second both in experiment [33,34], and simulation.[29] In particular, in the case of two contacting solid crystalline surfaces, the degree of commensurability has been shown to have a clear effect on friction.[2,35,36] Understanding the effect of these atomic interactions on energy loss will lend insight into the underlying mechanisms of friction. We have established the ability to tune the commensurability of a nanometer contact through AFM manipulation, providing a powerful knob to turn in performing experiments probing the origins of friction. Furthermore, we have established

that the electronic transport across the nanometer contact is also modulated smoothly as a function of commensurability.[37] This gives us an independent measure of the structure of the contact and a direct look at the relationship between mechanical and electronic processes in a sliding contact.[29]

When an AFM tip pushes an object, three types of motion can occur: uniform translation, rotation in the plane, and rolling. We have studied all three of these outcomes in the nanotube/flat substrate system. In the simplest case, the nanotube does not roll. Instead, it translates with a rotation in the plane. This is the behavior for multiwall nanotubes on substrates such as mica, oxidized silicon and MoS_2, and for graphite when the lattices are not interlocked. We have analyzed this motion with a simple analytical model that uses the AFM tip as a positional constraint, with a uniform distributed frictional force applied along the tube by the substrate. When the nanotube is manipulated from the side, the tube undergoes an in-plane rotation about a pivot point that depends on the location of the AFM tip during the push. A unique relation between the point of manipulation and the point of rotation can be derived with no fitting parameters, assuming a uniform friction along the length of the contact.[38] Additional phenomena emerge during end-on pushing of nanotubes. In this case, the lateral force shows a large initial spike before the onset of the uniform translation of the tube, a signature of stick-slip phenomena. These measurements have been shown to be consistent with the shear stress of a graphene sheet contact, demonstrating that the manipulation of surface bound objects can provide quantitative measures of the fundamental quantity of tribology, the surface shear stress, and do it for any combination of available nanoscale material and substrate while observing complex dynamics.

The manipulation of nanotubes reveals surprises when performed on graphite. If the nanotube starts in an out-of-registry state, it slides smoothly, as described above. However, this in-plane rotational motion is interrupted at discrete in-plane orientations where the nanotube "locks" into a low energy state, indicated by a ten-fold increase in the force required to move the CNT (Figure 4, left). Subsequently, the nanotube rolls with a constant in-plane orientation and characteristic stick-slip modulation in the lateral force.[39,40] This is shown in Figure 5 where manipulations from different nanotubes are shown. The characteristic of the rolling motion is a) no in-plane rotation during the translation of the CNT (as is observed in the non-graphitic substrates above), b) features in the topography (shape) of the nanotube that reappear in subsequent images, and c) features in the lateral force that reproduce themselves with a distance that corresponds to the circumference of the nanotube. The lateral force traces all show the expected periodic behavior, while the inset shows a set of images of the changing end cap of the nanotube upon manipulation. This sequence is repeated as the nanotube continues to be rolled across the substrate.

Why does the nanotube roll on graphite and not on other substrates? Most significant, nanotubes can be manipulated to reveal a set of three distinct in-registry orientations separated by 60+/-1 degrees. This behavior is seen in Figure 4(a) where we show lateral force traces as a CNT is rotated into (left trace) and out of (right trace) commensurate contact. The inset shows a top-view schematic the process for the left trace. (1) The AFM tip is moving along in contact with the graphite substrate. (2) The CNT is contacted and begins rotating in-plane (3). (4) The commensurate state is reached (indicated by the dashed line) and the lateral force rises dramatically before rolling

motion begins (5). The right trace begins with the tip on the substrate, the tip then contacts the CNT in the commensurate state, begins rolling and then pops out of commensurate contact and begins rotating in plane with a corresponding drop in lateral force. The AFM image sequence of Figure 5(a)-(c) shows a CNT in three manipulated commensurate orientations. The NT on the left of Figure 6(a), (b), and (c) is rotated in-plane into three commensurate orientations indicated by pronounced increase in lateral force as shown in Figure 4. In Figure 6(d), the three images were overlain to emphasize the 3-fold symmetry of the commensurate orientations. This set of manipulations and quantitative measurements show that the atomic arrangement of the substrate is responsible for the rolling behavior. Do the atoms of the nanotube play any role?

We have also manipulated two CNT's (CNT 1- 950nm long, 20nm diameter, CNT2- 500nm long, 34nm diameter) lying in the same immediate area on the graphite substrate. While each nanotube shows the complete set of lock-in behaviors noted above, the two CNT have lock-in orientations that are different from each other by 11 degrees. This difference in lock-in angles implicates the nanotube lattice in nanotube rolling. If the registered orientations are due to atomic registry, the particular set of registered orientations is determined by the nanotube chirality (the wrapping orientation of the outer graphene sheet of the CNT). Taken together, these two experiments imply that the atomic lattices are interlocking to produce rolling. The atoms can act like gear teeth. We have manipulated two CNT into a collision to demonstrate the robust gear-like motion (Figure 7). The orientation of each nanotube is preserved through the collision and subsequent rolling. The lateral force trace after the collision is the sum of the two periodic rolling signals from the individual CNT's (Figure 7, right).

Molecular statics and dynamics calculations have shed light on the rolling dynamics.[41,42] They have shown the discrete lock-in orientations, calculated energy barriers for sliding, in-plane rotation and rolling, all as a function of the nanotube size. Most important is our convergence on an explanation of our rolling data. Our results are consistent with faceted graphene cylinders. First, the lateral force traces are periodic with repeat distance equal to the nanotube circumference. Second, the molecular statics calculations on perfect cylinders indicate that the nanotube should always roll, as rolling has a lower energy barrier than any other motion, whether the tube is in-registry or out. The molecular statics calculations that allow relaxation of the nanotube shape show that a sufficiently large multiwall nanotube is faceted. We believe that this faceting plays a key role in our experimental observations. First, the energy cost for rolling now includes a component due to the adhesion of the facet face and the substrate, substantially larger than that for the perfect cylinder. This energy cost for rolling is lower than the energy cost of sliding only when the nanotube is in registry.

3.3 NANOSCALE CONTACTS: MOMENTUM CONSERVATION ACROSS A LATTICE PLANE CONTACT

The lattice plays a critical role in the transport of electrons across an interface. The ability to control the registry angle between the nanotube and the graphite substrate provides us the opportunity to study the electron transport dependence on the orientation of the crystalline axis in the contact. We have measured the resistance of the CNT/graphite contact via a two probe measurement: the graphite substrate itself serving as one lead, and a conducting AFM tip brought to contact the top of the CNT is the

other.[37] Resistance measurements as a function of lattice angle between the nanotube and the graphite substrate are taken in the following manner. The NT is imaged in non-contact (oscillating) mode to locate the tube and measure the angle of the tube. The zero of angle for each tube, designated as the commensurate position, is determined by the lateral force signal that shows the lock-in position. The tip is then engaged in contact mode on top of the NT with the desired force (~50 nN), and the voltage between the tip and sample is swept from -0.1 to 0.1 V while the current is measured. Data for two different tubes are shown in Figure 8. Data from a tube that has been rotated through 180 degrees, with resistance measurements taken approximately every seven to ten degrees is shown in Figure 8 (top). From the data, it is clear the resistance minima occur at the commensurate positions- 0, 60, 120 and 180 degrees, and that the data is periodic, repeating every sixty degrees. Figure 8 (bottom) shows more dense data, collected approximately every 3 degrees from a different CNT (45 nanometers by 1.6 microns) showing in detail the change in the resistance near the commensurate position.

An analysis of the resistance measurements for the tip against the nanotube and directly applied to the substrate allows us to conclude that the nanotube-graphite contact resistance is changing by a factor of fifty, with the lowest resistance occurring in the in-registry orientation, when the nanotube and substrate have the A-B stacking of crystalline graphite. Why is the resistance lowest in this orientation? Two possible answers are the effect of atomic interlocking and the conservation of momentum. The first has been studied by calculations that show a change in the contact resistance by a factor of two as two single wall nanotubes are translated past each other.[43] This implies that the conservation of k-vector, the direction of the wavefunction, is the dominant effect in our

measurements. The conduction electrons in graphite are located at the corners of the hexagonal Brilloiun zone, meaning that there are six allowed directions for the electron transport.[44,45] The contact resistance will be lowest when the wavefunctions in the nanotube and in the substrate have the same value of the k-vector, including direction, and therefore allow transport from one to the other without additional scattering. Therefore, the ability to manipulate the top contact in an atomically clean junction has allowed the striking demonstration of a fundamental concept in transport, momentum conservation. This implies that devices based on nanotubes will need to control the relative lattice orientations, or take advantage of this dependence for a new class of sensors and devices.

3.4 NANOMANIPULATION AND MEMS DEVICES

The correlation of structure and properties is the cornerstone of the physical sciences, and the design and control of the nanoworld depends on measurements performed simultaneous with atomic scale structure determination. The tool of choice for atomic scale structure has been high-resolution transmission electron microscopy (TEM). While the TEM can provide atomic scale chemical information, the space within the microscope is extremely tight, with sample volumes less than a few millimeters thick. This presents a significant challenge to the design of mechanical stressing stages and force sensing manipulation stages that can be integrated with the TEM. We have begun to design such stages using Microelectromechanical Systems (MEMS) technology that is being widely applied in sensing systems, displays and optoelectronics.[46,47] This technology can be used to create moving stages with manipulation capability, as well as

force and transport sensing stages for correlated stress/strain/transport/structure measurements. With such stages in hand, the remaining challenge is to place the nanostructure of interest into the device. We have succeeded in using our SEM/AFM manipulation system to place carbon nanotubes onto MEMS stages, and to use stages designed for stress-strain measurements to grab nanotubes.

The methodology, shown in Figure 9, starts with the creation of a nanotube cartridge through electro-deposition of nanotubes onto the edge of a metal foil from a nanotube/dichloromethane suspension.[48] The nanotubes protrude off the edge of the foil and act as a source for manipulation by the AFM tip. The tip is positioned against the nanotubes and it is observed that Van der Waals forces are sufficient to adhere them to the silicon AFM tip and pull the tubes away from the foil. The nanotube is clearly observed in the SEM image during the positioning of the tip and the pull-off. The AFM tip is then positioned over the gap in the MEMS device and the contact of the nanotube is observed as it begins to bend. The tip is then moved laterally across the gap, laying the tube down on the near edge of the device. The SEM is then made to image the location where the CNT lies flat against the surface, depositing a carbon contamination layer that can pin the nanotube and provide electrical contact.[49] The tip is then moved further away until the CNT drops completely off of the tip and lies on the far side of the gap. The SEM is then again used to tie the CNT to the surface. Carbon contamination layer produced by the electron bombardment has been shown to be sufficient to secure the nanotube even under stresses that tore the CNT. This methodology of nanosample placement on MEMS testing structures will allow subsequent use of the MEMS test stage in a variety of

settings, such as TEM or low temperature, high magnetic field cryostats where in-situ manipulation is very challenging.

We have also demonstrated that MEMS stages can be used to grab nanosamples during the manipulation of CNT. In this experiment, shown in Figure 10, the nanotube, as attached to an AFM tip, was positioned in the gap of a MEMS stress/strain stage. The stage was then closed through the actuation of the comb drive. The tip was then retracted until the nanotube was observed to sever. Transport measurements were taken during the manipulation and the application of stress, and they showed significant changes during the stretching of the CNT. These measurements will be improved by a post-processing step of metalization to provide a metal-nanotube junction within the MEMS device. The ability to manipulate nanoscale structures provides great flexibility in characterization methodologies, including the application of integrated testing stages that can be incorporated into the tight confines of high-resolution transmission electron microscopes and low temperature cryostats.

3.5 NANOMANIPULATION IN BIOLOGY: BINDING AND DYNAMICS

The study of surface interactions and dynamics of biological macromolecules and macromolecular assemblies will provide insight into specific binding that may occur at cell surfaces and the transport of vesicles and viruses. The application of normal forces to measure the energetics of macromolecule extension and antibody-antigen binding has been pursued using AFM.[50,51] Here we discuss the application of lateral forces to measure surface interactions and dynamics of viruses.[52,53] The force necessary to move a virus across the surface can reveal specific and non-specific interactions, and potentially,

through the use of molecularly treated surfaces, probe model cell membrane substrates. In addition, the translation of viruses within the lumen of vessels or on the cell surface is not understood. The measurement of lateral forces during manipulation can shed light on the mode of transport: rolling or sliding.

We have performed preliminary measurements of virus manipulation on solid surfaces under ambient conditions. Our target virus is adenovirus, of interest as a human pathogen and as a vector for gene therapy.[54] Adenoviruses have been deposited onto clean and functionalized silicon substrates, with manipulations performed in liquid and in air under low humidity conditions. While it is clear that measurements performed in liquid will provide the most direct insight into physiological processes,[55] measurements performed in air are relevant to viral delivery strategies that require the drying of the virion for storage and dosage. Figure 11 shows a typical manipulation under ambient conditions, with an initial large manipulation force needed to dislodge the virus before its first translation, with a subsequent low force needed to maintain its motion. A second push has a much lower force to initiate motion. We believe that the initial peak is indicative of the strength of surface binding of the virus with subsequent pushes placing a virion surface in contact with the substrate that is unable to relax to minimize the interfacial energy.

A closer examination of the lateral force traces reveals insight into the mode of virus transport during manipulation. The autocorrelation of the lateral force during manipulation, shown in Figure 12, reveals a periodicity in the lateral force of 23.5 nm. The virion, with an icosahedral shape has a height of 75nm, and a circumference of 235 nm across ten faces.[56] This corresponds to the periodicity in the lateral force trace, and

reveals a peeling process that is occurring as the virion is rolled from face to face as it is manipulated across the surface. Manipulation of control particles, spherical polystyrene bead of similar diameter, showed no signature of periodicity.

The case of the virus bears similarities and differences from the case of carbon nanotubes. Both reveal rolling through a periodicity in the lateral force trace that is consistent with the geometrical features of the object. However, we found that the nanotube involved a balance between sliding and peeling energies that dictated that the nanotube should roll unless the sliding energy was increased through commensurate contact with a substrate. However, the virus was observed to roll on homogeneous substrates where no gear-like interlocking could occur. The molecular origins of the virus/substrate interactions, and the competition between sliding and peeling (rolling) await to be uncovered.

4. CONCLUSION

The strongest material buckling like a soda straw, atomic teeth as gears, electron transport facilitated by the interlocking of atomic lattices, rolling viruses. There is much to be learned about the nanoscale world, including how properties such as electrical transport, mechanical properties and dynamics are affected by the atomic scale structure of the nano-objects and their interfaces. Nanomanipulation provides exciting insight into these problems by allowing us to probe individual objects with great facility, and to combine property characterization with structural information. Advanced user interfaces will continue to play a critical role in making experiments more transparent to the user, and enabling the scientist to be an actor in the nanoscale world.

Acknowledgements: The authors would like to thank the members of the NanoScience Research Group at UNC for their work, and the National Science Foundation, the National Institutes of Health National Center for Research Resources, the Office of Naval Research and the Army Research Office for support.

References

[1.] Guntherodt, H.-J., Anselmetti, D., and Meyer, E., Forces in Scanning Probe Methods, in *NATO ASI series. Series E, Applied Sciences*, 1st. ed. Kluwer Academic Publishers, Dordrecht, The Netherlands, 1995.

[2.] Sheehan, P. E. and Lieber, C. M., Nanotribology and Nanofabrication of $Mo0_3$ Structures by Atomic Force Microscopy, *Science* 272 (May 24), 1158 - 1161, 1996.

[3.] Luthi, R., Meyer, E., Haefke, H., Howald, L., Gutmannsbauer, W., and Guntherodt, H.-J., Sled-Type Motion on the Nanometer Scale: Determination of Dissipation and Cohesive Energies of C_{60}, *Science* 266 (December 23), 1979 - 1981, 1994.

[4.] Resch, R., Baur, C., Bugacov, A., Koel, B. E., Madhukar, A., Requicha, A. A. G., and Will, P., Building and manipulating three-dimensional and linked two- dimensional structures of nanoparticles using scanning force microscopy, *Langmuir* 14 (23), 6613-6616, 1998.

[5.] Postma, H. W. C., de Jonge, M., Yao, Z., and Dekker, C., Electrical transport through carbon nanotube junctions created by mechanical manipulation, *Physical Review B* 62 (16), R10653-R10656, 2000.

[6.] Williams, P. A., Patel, A. M., Papadakis, S. J., Seeger, A., Taylor II, R. M., Helser, A., Sinclair, M., Falvo, M. R., Washburn, S., and Superfine, R., Controlled placement of an individual carbon nanotube onto a MEMS structure, *Appl. Phys. Lett.*, 2574-2576, 2002.

[7.] Taylor II, R. M. and Superfine, R., Advanced Interfaces to Scanning Probe Microscopes, in *Handbook of Nanostructured Materials and Nanotechnology*, Nalwa, H. S. Academic Press, New York, 1999, pp. 271-308.

[8.] Falvo, M. R., Clary, G., Helser, A., Paulson, S., Taylorr II, R. M., Chi, V., Brooks Jr., F. P., Washburn, S., and Superfine, S., Nanomanipulation experiments exploring frictional and mechanical properties of carbon nanotubes, *Microsc. Microanal.* 4, 504-512, 1998.

[9.] Guthold, M., Falvo, M., Matthews, W. G., Paulson, S., Mullin, J., Lord, S., Erie, D., Washburn, S., Superfine, R., Brooks, F. P., and Taylor, R. M., Investigation and Modification of Molecular Structures Using the NanoManipulator, *J Mol. Graph. Model.* 17, 187-197, 1999.

[10.] Magonov, S. N. and Whangbo, M.-H., *Surface Analysis with STM and AFM : Experimental and Theoretical Aspects of Image Analysis* VCH Publishers Inc., New York, 1996.

[11.] Bonnell, D. A., Scanning Probe Microscopy and Spectroscopy : Theory, Techniques, and Applications, Wiley, New York, 2000.

[12.] Weigle, C., Emigh, W. G., Liu, G., Taylor II, R. M., Enns, J. T., and Healey, C. G., Oriented Sliver Textures: A Technique for Local Value Estimation of Multiple Scalar Fields, in *Proc. Graphics Interface 2000*, Montreal, Canada, 2000.

[13.] Seeger, A., Henderson, A., Pelli, G. L., Hollins, M., and Taylor II, R. M., Haptic Display of Multiple Scalar Fields on a Surface, in *Proceedings of the Workshop on New Paradigms in Information Visualization and Manipulation, NPIVM 2000*, Washington, D.C., 2000, pp. 33-38.

[14.] Falvo, M., Finch, M., Chi, V., Washburn, S., Taylor II, R. M., Brooks Jr., F. P., and Superfine, R., The Nanomanipulator: A Teleoperator for Manipulating Materials at the Nanometer Scale, in *Proceedings of the 5th International Symposium on the Science and*

Engineering of Atomically Engineered Materials World Scientific, Richmond, VA, November 5, 1995.

[15.] Seeger, A., Paulson, S., Falvo, M., Helser, A., Taylor II, R. M., Superfine, R., and Washburn, S., Hands-on tools for nanotechnology, *J. Vac. Sci. Technol. B* 19, 2717-2722, 2001.

[16.] Iijima, S., Helical microtubules of graphitic carbon, *Nature* 354, 56-58, 1991.

[17.] Thess, A., Lee, R., and Smalley, R. E., Crystalline ropes of metallic carbon nanotubes, *Science* 273 (July 26), 483, 1996.

[18.] Ebbesen, T. W. and Ajayan, P. M., Large scale synthesis of carbon nanotubes, *Nature* 358, 16, 1992.

[19.] Dresselhaus, M. S., Dresselhaus, G., and Avouris, P., Carbon Nanotubes: Synthesis, Structure, Properties and Applications, Springer, New York, 2001.

[20.] Wong, E. W., Sheehan, P. E., and Lieber, C. M., Nanobeam mechanics: elasticity, strength, and toughness of nanorods and nanotubes, *Science* 277, 1971-1975, 1997.

[21.] Treacy, M. M. J., Ebbesen, T. W., and Gibson, J. M., Exceptionally high Young's modulus observed for individual carbon nanotubes, *Nature* 381 (June 20), 678-680, 1996.

[22.] Falvo, M. R., Clary, G. J., Taylor, R. M. I., Chi, V., Brooks, F. P. J., Washburn, S., and Superfine, R., Bending and buckling of carbon nanotubes under large strain, *Nature* 389 (October 9), 582-584, 1997.

[23.] Pizer, S. M., Eberly, D., Morse, B. S., and Fritsch, D. S., Zoom-invariant vision of figural shape: the mathematics of cores, *Computer Vision and Image Understanding*, 1997.

[24.] Poncharal, P., Wang, Z. L., Ugarte, D., and de Heer, W. A., Electrostatic deflections and electromechanical resonances of carbon nanotubes, *Science* 283 (March 5), 1513-1516, 1999.

[25.] Bower, C., Rosen, R., Jin, L., Han, J., and Zhou, O., Deformation of carbon nanotubes in nanotube-polymer composites, *Applied Physics Letters* 74 (22), 3317-3319, 1999.

[26.] Ju, G. T. and Kyriakides, S., Bifurcation and localization instabilities in cylindrical shells under bending - II. Predictions, *Int. J. Solids Structures* 29 (9), 1143-1171, 1992.

[27.] Axelrad, E. L., On local buckling of thin shells, *Int. J. Non-Linear Mechanics* 20 (4), 249-259, 1985.

[28.] Bhushan, B., Micro/Nanotribology and Micro/Nanomechanics of MEMS Devices, in *Micro/Nano Tribology*, Bhushan, B. CRC Press, New York, 1998, pp. 797.

[29.] Persson, B. N. J., *Sliding Friction: Physical Principles and Applications* Springer-Verlag, Berlin, 1998.

[30.] Israelachvili, J., *Intermolecular and Surface Forces*, 2 ed. Academic Press, San Diego, 1991.

[31.] Johnson, K. L., A continuum mechanics model of adhesion and friction in a single asperity contact, in *Micro/nanotribology and its applications*, Bhushan, B. Kluwer Acadmenic Publishers, Dordrecht, The Netherlands, 1997, pp. 157.

[32.] Mate, M. C., McClelland, G. M., Erlandsson, R., and Chiang, S., Atomic-scale friction of a tungsten tip on a graphite surface, *Phys. Rev. Lett.* 59 (17), 1942-1945, 1987.

[33.] Overney, R. M., Takano, H., Fujihira, M., Paulus, W., and Ringsdorf, H., Anisotropy in friction and molecular stick-slip motion, *Phys. Rev. Lett.* 72 (22), 3546-3549, 1994.

[34.] Liley, M., Gourdon, D., Stamou, D., Meseth, U., Fischer, T. M., Lautz, C., Stahlberg, H., Vogel, H., Burnham, N. A., and Duschl, C., Friction anisotropy and asymmetry of a compliant monolayer induced by a small molecular tilt, *Science* 280, 273-275, 1998.

[35.] He, G., Muser, M. H., and Robbins, M. O., Adsorbed layers and the origin of static friction, *Science* 284 (4 June), 1650-1652, 1999.

[36.] Hirano, H., Shinjo, K., Kaneko, R., and Murata, Y., Anisotropy of frictional forces in muscovite mica, *Phys. Rev. Lett.* 67 (19), 2642-2645, 1991.

[37.] Paulson, S., Falvo, M., Buongiorno Nardelli, M., Taylor II, R. M., Helser, A., Superfine, R., and Washburn, S., Tunable resistance of a carbon nanotube-graphite interface, *Science* 290, 1742-1744, 2000.

[38.] Mason, M. T. and Salisbury , J. K. J., *Robot Hands and the Mechanics of Manipulation* MIT Press, Cambridge, MA, 1985.

[39.] Falvo, M. R., Taylor II, R. M., Helser, A., Chi, V., Brooks Jr. , F. P., Washburn, S., and Superfine, R., Nanometre-scale rolling and sliding of carbon nanotubes, *Nature* 397 (21 January), 236-238, 1999.

[40.] Falvo, M., Steele, J., Taylor II, R. M., and Supefine, R., Gearlike rolling motion mediated by commensurate contact: Carbon nanotubes on HOPG, *Phys. Rev. B.* 62, R10665-10667, 2000.

[41.] Schall, J. D. and Brenner, D. W., Molecular dynamics simulations of carbon nanotube rolling and sliding on graphite, *Molecular Simulation* 25 (1-2), 73-79, 2000.

[42.] Buldum, A. and Lu, J. P., Atomic scale sliding and rolling of carbon nanotubes, *Phys. Rev. Lett.* 83 (24), 5050-5053, 1999.

[43.] Buldum, A. and Lu, J. P., Contact resistance between carbon nanotubes, *Phys. Rev. B* 63, 161403-161406, 2001.

[44.] Mintmire, J. W., Dunlap, B. I., and White, C. T., Are Fullerenes Metallic, *Phys. Rev. Lett.* 68, 631, 1992.

[45.] Dresselhaus, M. S., Dresselhaus, G., and Eklund, P. C., *Science of Fullerenes and Carbon Nanotubes* Academic Press, San Diego, 1996.

[46.] Craighead, H. G., Nanoelectromechanical systems, *Science* 290, 1532-1535, 2000.

[47.] Bishop, D., Gammel, P., and Randy Giles, C., The little machines that are making it big, *Physics Today* 54 (10), 38-44, 2001.

[48.] Nishijima, H., Kamo, S., Akita, S., Nakayama, Y., Hohmura, K. I., Yoshimura, S. H., and Takeyasu, K., Carbon-nanotube tips for scanning probe microscopy: Preparation by a controlled process and observation of deoxyribonucleic acid, *Applied Physics Letters* 74 (26), 4061-4063, 1999.

[49.] Yu, M. F., Files, B. S., Arepalli, S., and Ruoff, R. S., Tensile loading of ropes of single wall carbon nanotubes and their mechanical properties, *Physical Review Letters* 84 (24), 5552-5555, 2000.

[50.] Wang, M. D., Manipulation of single molecules in biology, *Current Opinion in Biotechnology* 10 (1), 81-86, 1999.

[51.] Hansma, H. G. and Hoh, J., Biomolecular imaging with atomic force microscope, *Ann. Rev. Biophys. Biomol. Struct.* 23, 115-139, 1994.

[52.] Falvo, M. R., Washburn, S., Superfine, R., Finch, M., Brooks, F. P. J., Chi, V., and Taylor, R. M. I., Manipulation of individual viruses: friction and mechanical properties, *Biophys. J.* 72 (March), 1396-1403, 1997.

[53.] Matthews, G., Guthold, M., Negishi, A., Taylor, R. M., Erie, D., Jr., F. P. B., and Superfine, R., Quantitative manipulation of DNA and viruses with the nanoManipulator Scanning Force Microscope, *Surf. Interface Anal.* 27, 437-43, 1999.

[54.] Samulski, R. J., *Adeno-associated virus based vectors for human gene therapy.* World Scientific Publishing Co., Singapore, 1995.

[55.] Bustamante, C. and Keller, D., Scanning force microscopy in biology, *Physics Today* 48 (12), 32-38, 1995.

[56.] Horne, R. W., Brenner, S., Waterson, A. P., and Wildy, P., The icosahedral form of an adenovirus., *J. Mol. Biol.* 1, 84-86, 1959.

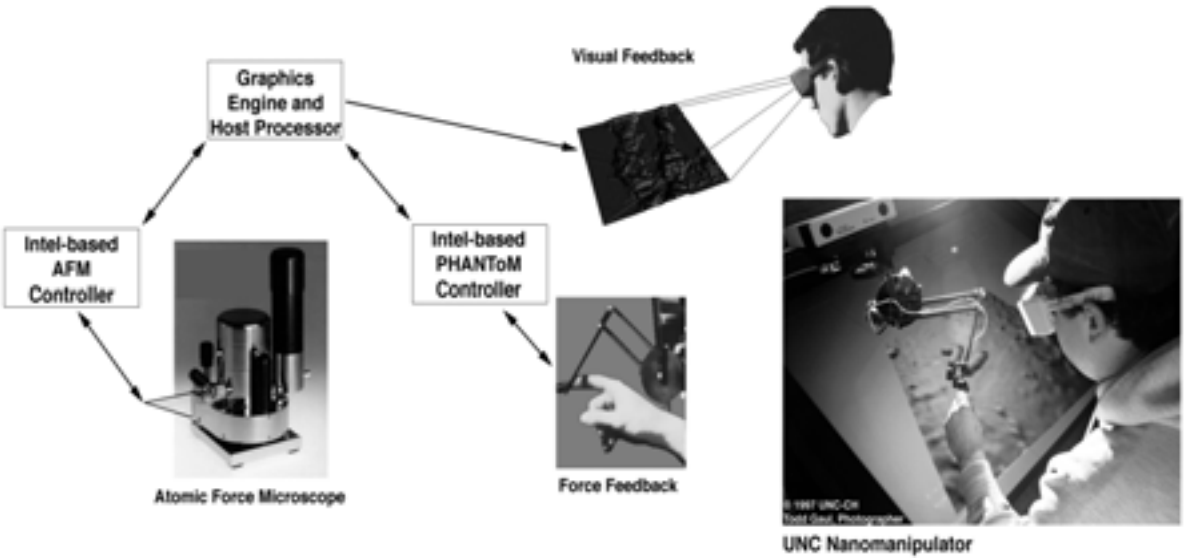

Figure 1.

Filename: Fig1.nMsystemDrawing.eps

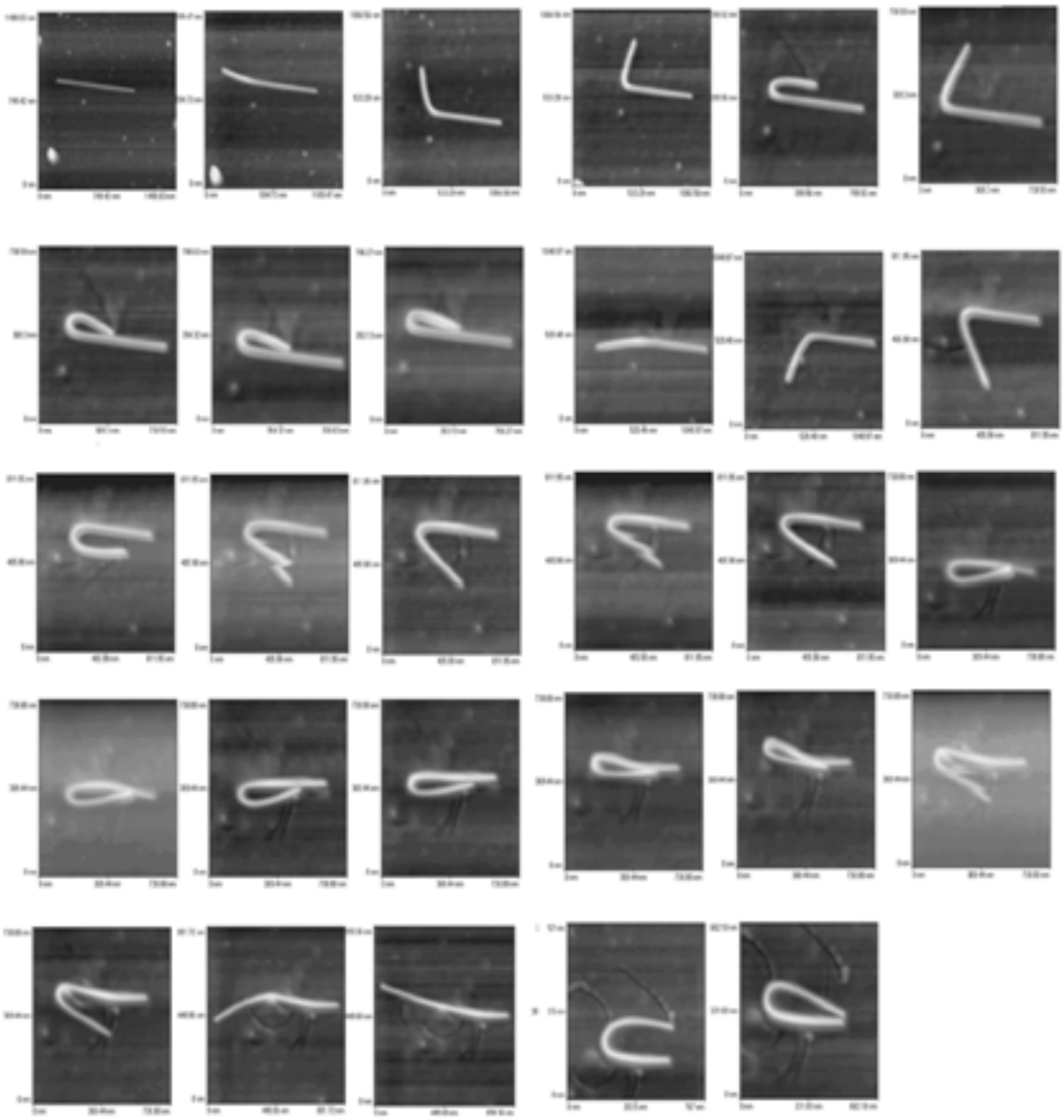

Figure 2.

Filename: Fig2.bendsequence.eps

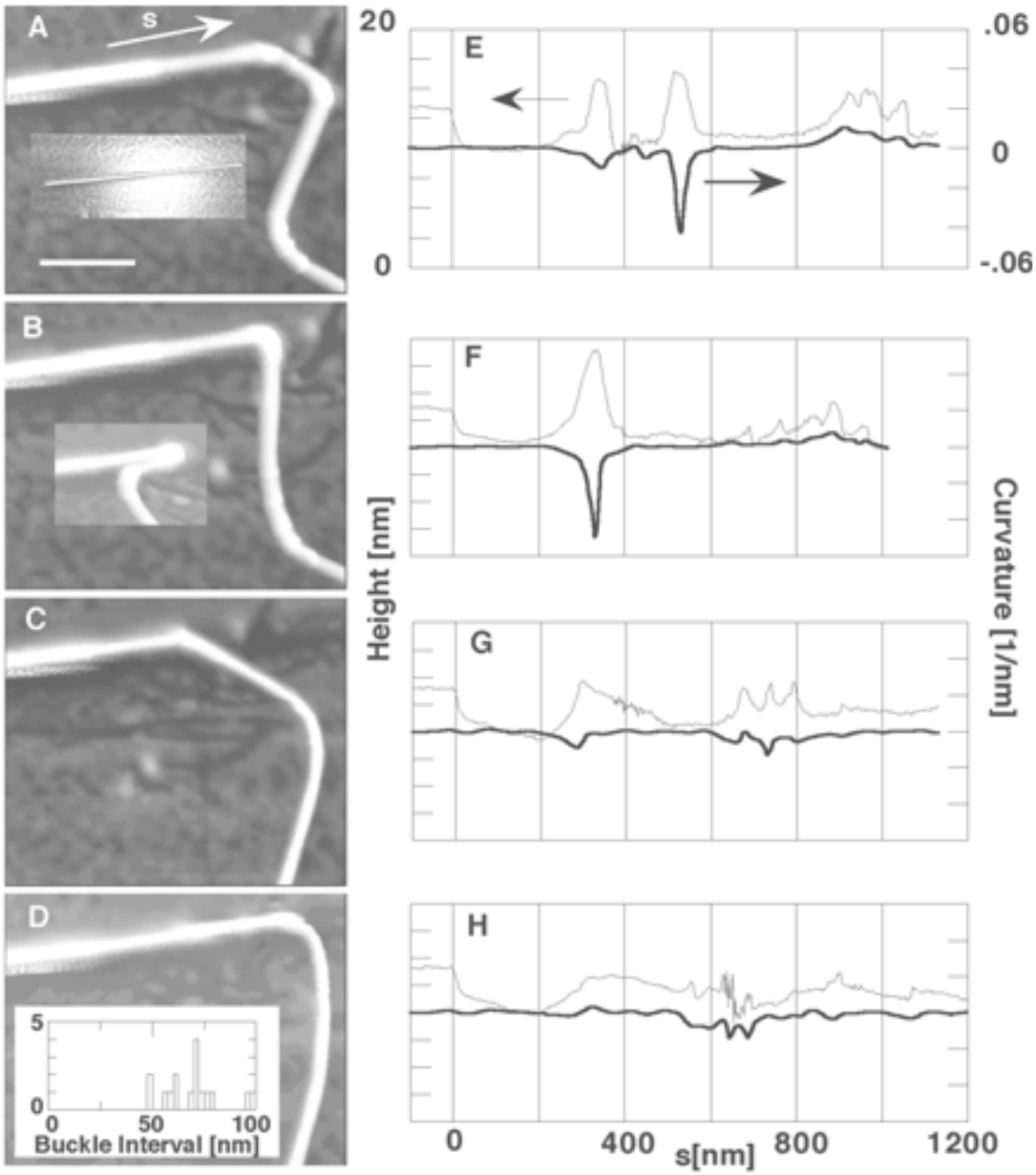

Figure 3

Filename: Fig3.bucklecomposite.eps

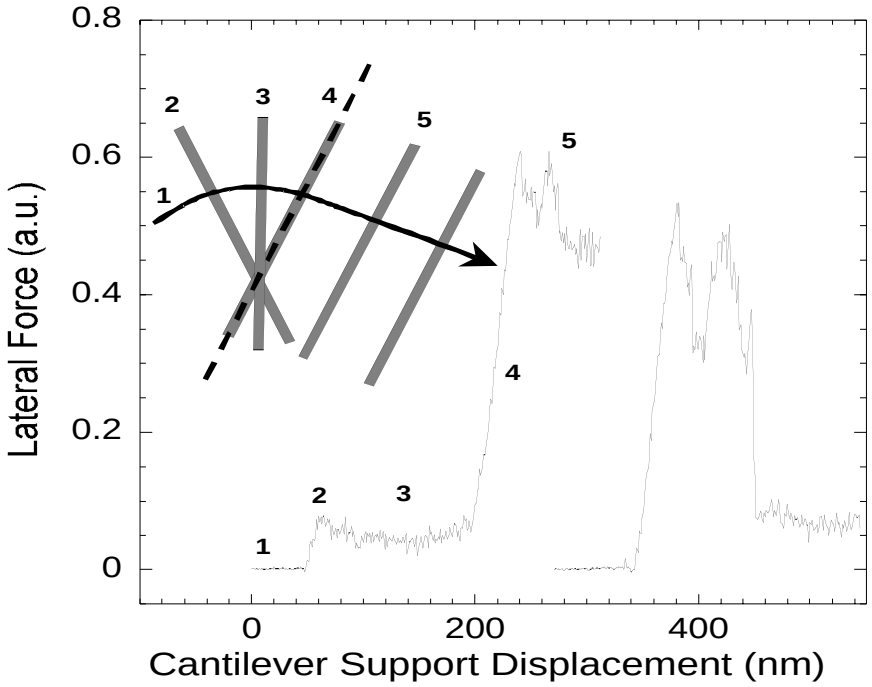

Figure 4

Filename: Fig4.RotateSlideCNT.eps

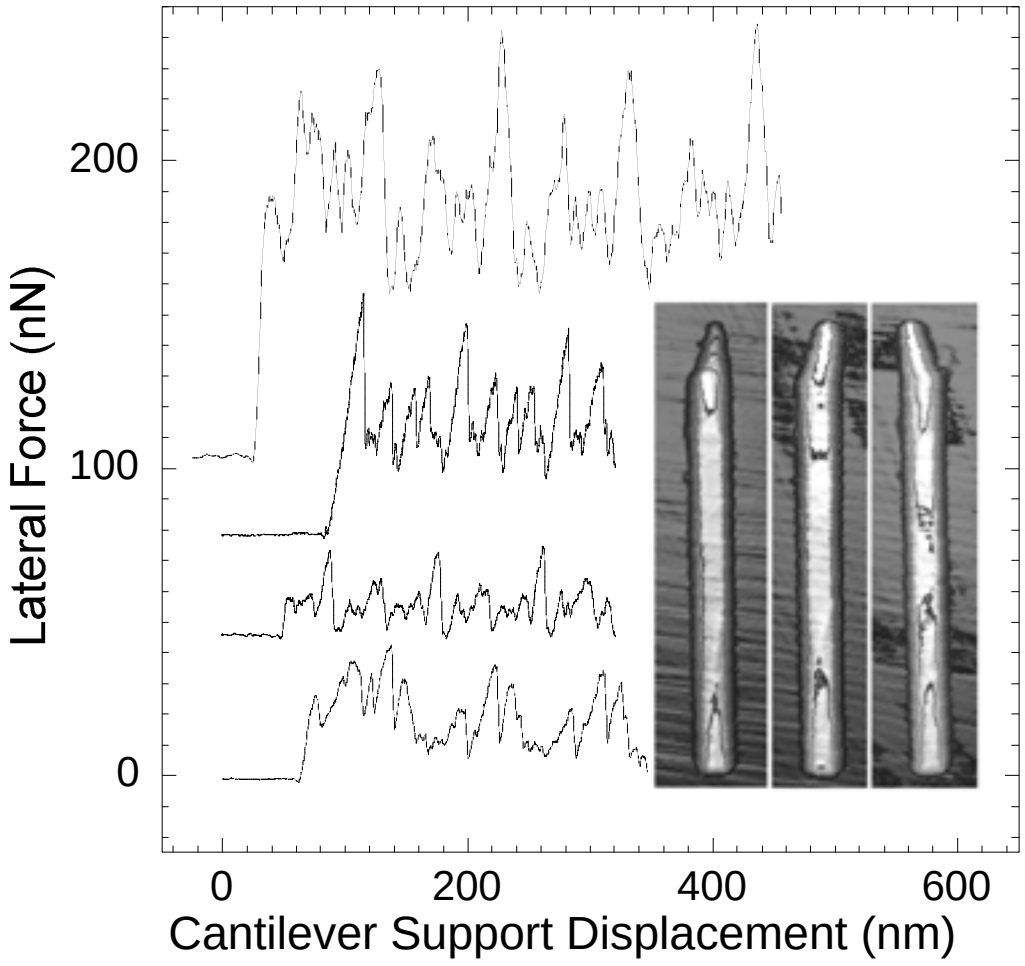

Figure 5

Filename: Fig5.RollCNT.eps

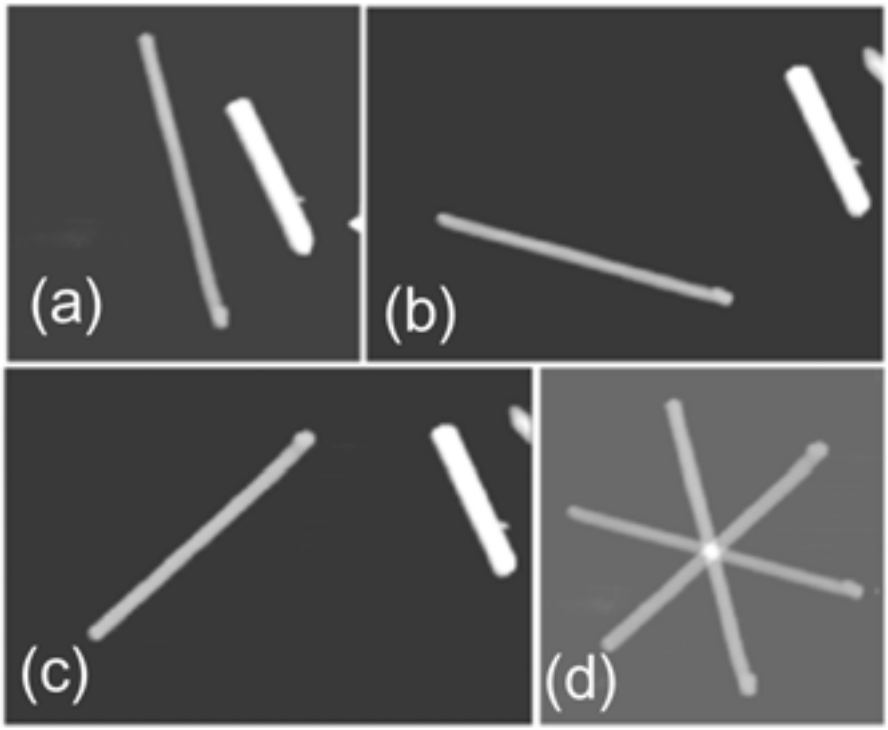

Figure 6

Filename: Fig6.rotatecomposite.CNT.eps

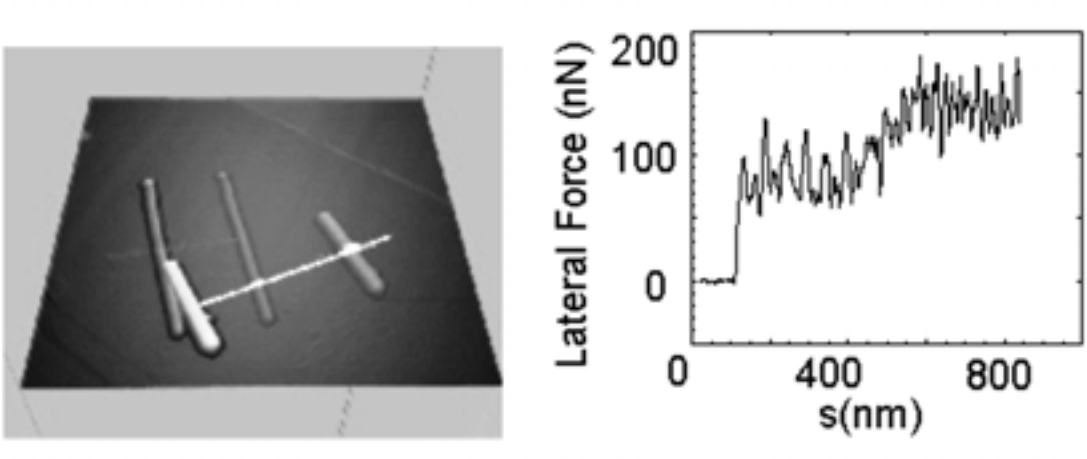

Figure 7

Filename: Fig7.collisonCNT.eps

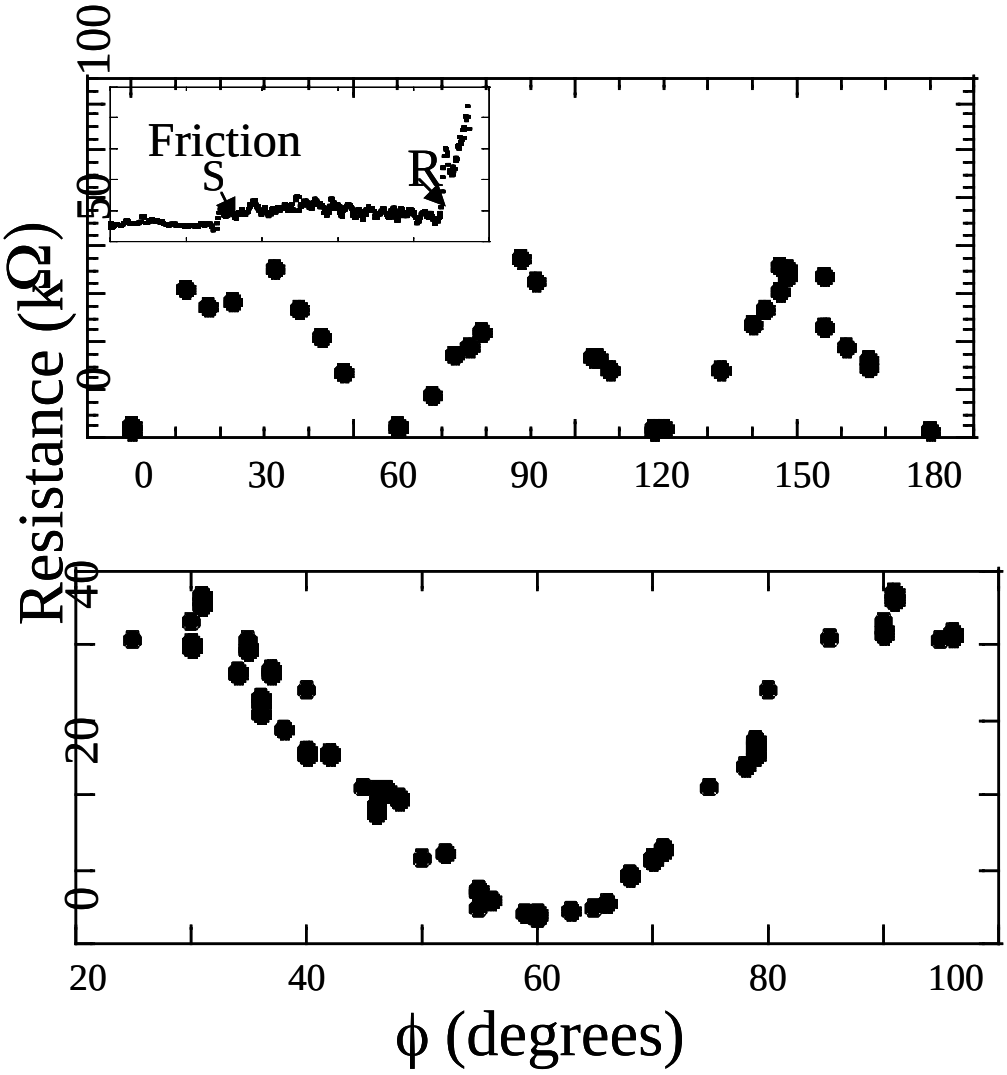

Figure 8

Filename: Fig8.nanoRheoPlots.eps

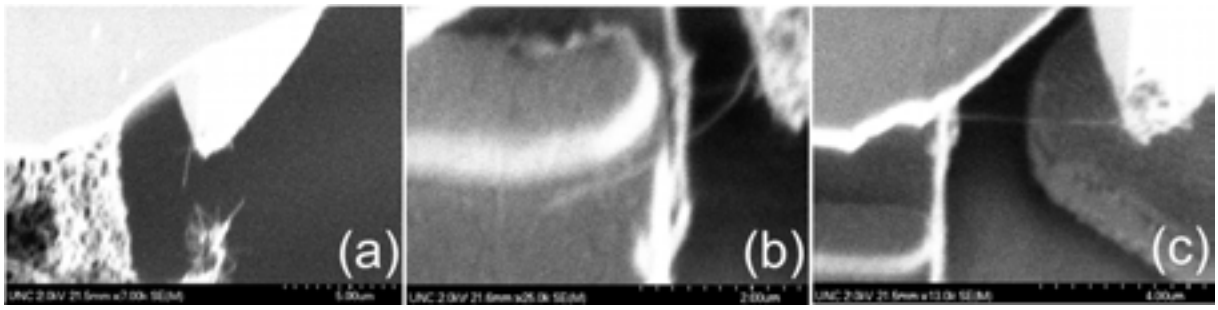

Figure 9

Filename: Fig9.MEMSCNT.eps

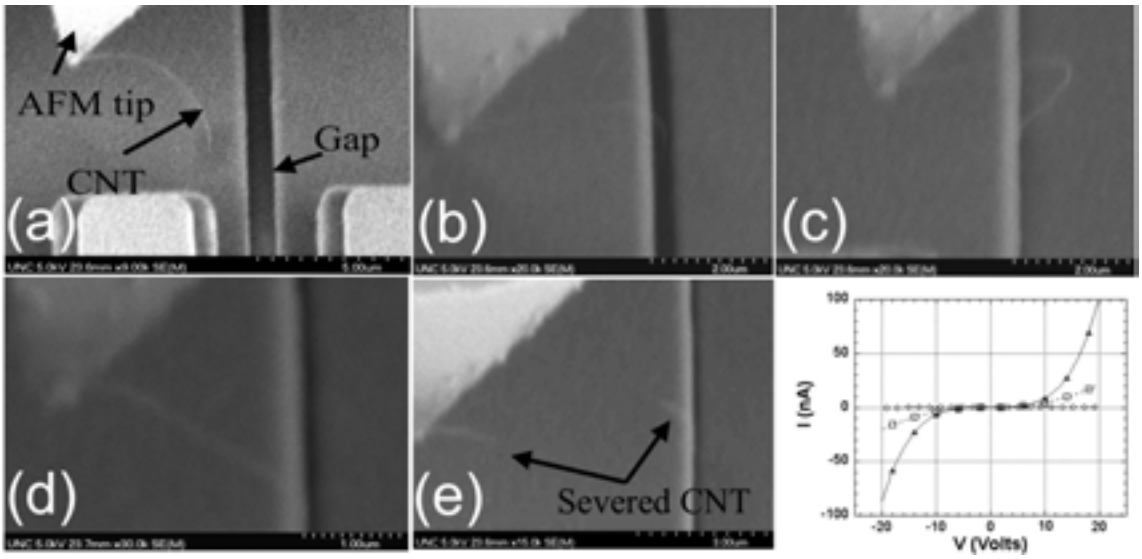

Figure 10

Figure Filename: Fig10.CNTMEMS.eps

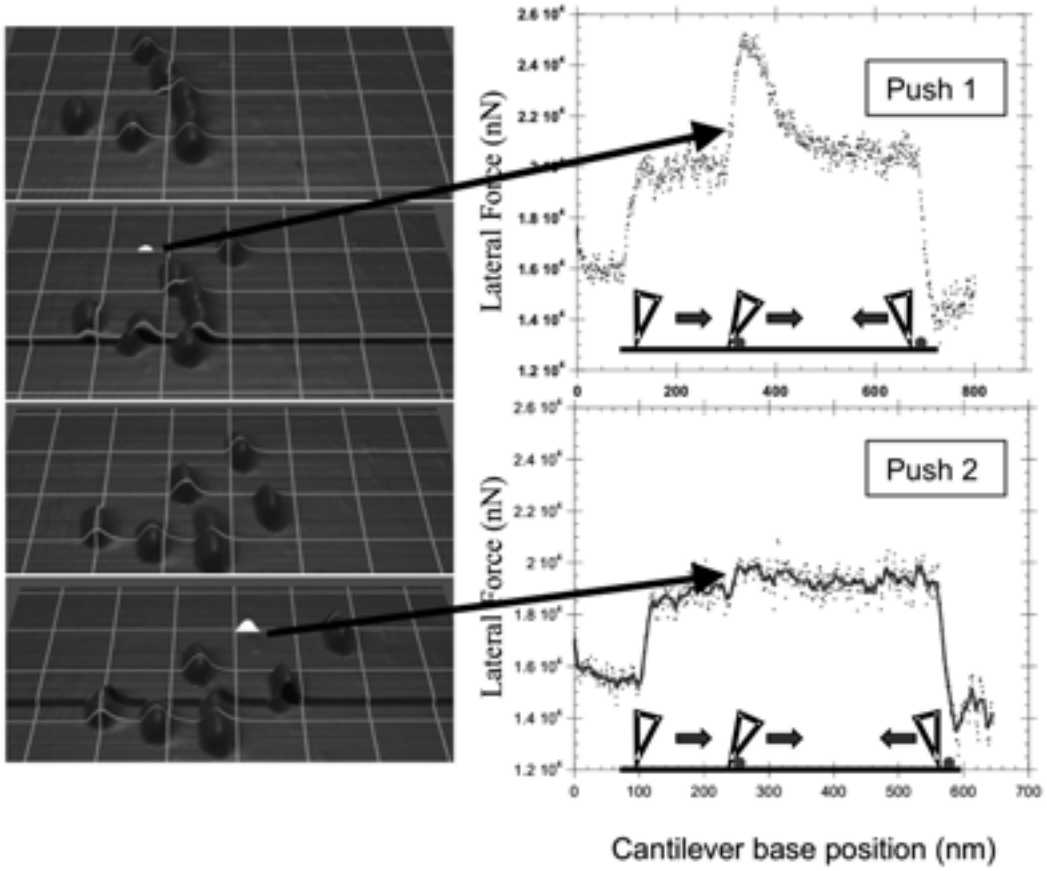

Figure 11

Filename: Fig11.adenoslide.eps

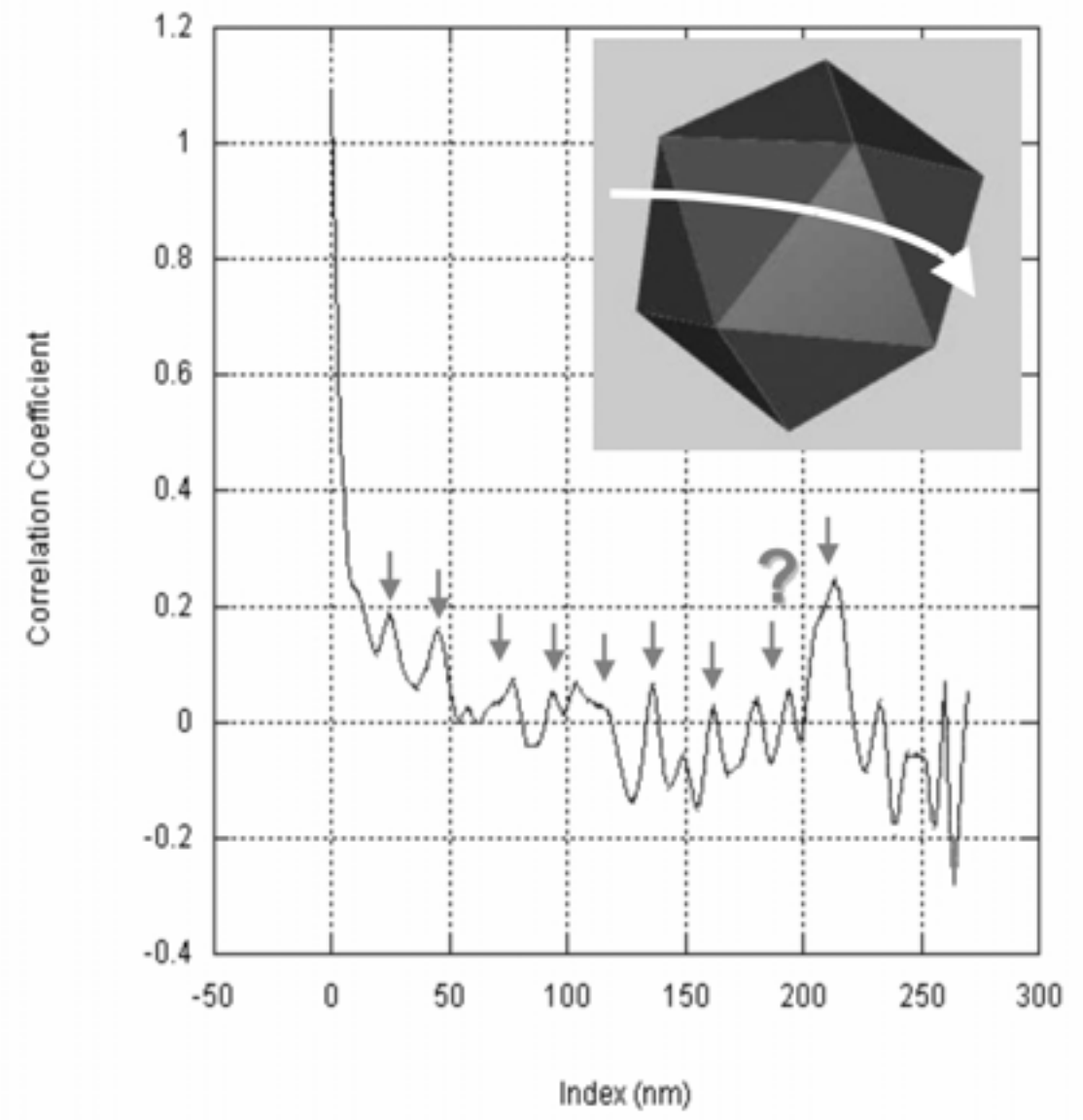

Figure 12

Filename: Fig12.adenoroll.eps

NANOMANIPULATION: BUCKLING, TRANSPORT AND ROLLING AT THE NANOSCALE

Figure Captions

Figure 1.

nanoManipulator system diagram with the system in use. The nanoManipulator comprises a scanning probe microscope (SPM) with its controller, a PHANToM force-feedback device with its controller and a PC computer with graphics card. These three computers communicate across an IP-based network. This system combines head-tracked stereo video with a force-feedback input device to allow the user to see and feel a 3D representation of the surface under study with an SPM. The user is in direct control of the tip's lateral motion and force, allowing him to manipulate the surface. This picture shows physics graduate student Scott Paulson using the system to investigate virus particles.

Figure 2.

A sequence of images of a carbon multiwall nanotube deposited on a silicon substrate manipulated by an atomic force microscope tip back and forth through strains as high as 16%. No catastrophic fracture of the nanotube is observed.

Figure 3.

Curvature and height of buckles along bent carbon nanotube. The white scale bar (A) is 300nm long and all figures are to the same scale. A 20nm diameter tube is manipulated

with AFM from its straight shape (inset of A) into several bent configurations (A-D). The height and curvature of the bent tubes along its centerline (indicated by the arrow in A) is plotted (E-H). The upper trace in each graph depicts the height relative to the substrate and the lower depicts the curvature data. The “ripple” like buckles occur between s= 600 nm and 1200nm and correspond to the tube in the lower right portion of the images in each case. Note that these buckles migrate as the tube is manipulated into different configurations. The appearance and disappearance of the ripple buckles as well as the severe buckle at s~500nm (E-F) suggest elastic reversibility. The distance between “ripple” buckles was determined for the various bent configurations of the experiment. The average of the buckle interval histogram (D, inset) establish the dominant interval as 68nm as the characteristic length of the rippling

Figure 4.

Lateral force trace as a carbon nanotube (CNT) is rotated into (left trace) and out of (right trace) commensurate contact. The inset shows a top-view schematic the process for the left trace. (1) The AFM tip is moving along in contact with the graphite substrate. (2) The CNT is contacted and begins rotating in-plane (3). (4) The commensurate state is reached (indicated by the dashed line) and the lateral force rises dramatically before rolling motion begins (5). The right trace begins with the tip on the substrate, the tip then contacts the CNT in the commensurate state, begins rolling and then pops out of commensurate contact and begins rotating in plane with a corresponding drop in lateral force.

Figure 5.

Periodic lateral force traces indicating rolling motion. The four traces are for four different CNT. In each case, the periodicity in the traces matches the circumference of the nanotube, indicating rolling without slipping motion. The inset illustrates the topographical evidence for rolling. The top end of the nanotube has an asymmetry that changes in a way that is consistent with rolling motion. The second trace from the top corresponds to the nanotube in the inset sequence.

Figure 6.

Commensurate orientations of a CNT on graphite. The nanotube on the left of (a), (b), and (c) is rotated in-plane into three commensurate orientations indicated by pronounced increase in lateral force as shown in Figure 4. In (d), the three images were translated and overlain to emphasize the 3-fold symmetry of the commensurate orientations. Similar measurements performed on the shorter CNT demonstrated a registry angle 11 degrees different from the longer tube, most clearly explained as a difference in the chirality of the nanotubes.

Figure 7.

The right (short) CNT is manipulated by the AFM tip to roll across the graphite substrate. The short CNT collides with the longer CNT and the two nanotubes continue to roll across the surface, each maintaining their own lock-in angles, with the AFM tip touching only the shorter CNT. The lateral force trace on the right shows a jump at 150 nm when the AFM tip touches the short CNT, and a second jump at 550 nm when the short CNT

begins to push (and roll) the longer CNT. The trace to the left of 550 nm shows the lateral force needed to roll both CNT at the same time.

Figure 8.

Measurement of electron transport through the atomic lattice contact of a CNT with a graphite substrate. The resistance of a two-probe measurement from a metallized AFM tip contacting the top of a CNT into the graphite substrate is plotted as a function of the registry angle. The lateral force signature of lattice registry determines the lock-in angles. The resistance is periodic, consistent with a CNT/graphite contact resistance that is 50 times smaller when the lattices are in registry. The lower trace is a higher angle resolution trace showing the detail as the lattices approach registry.

Figure 9.

Manipulation of nanotube onto MEMS device using combination SEM/AFM manipulation system for correlation of stress/strain and conductance of individual elements and nanotube/matrix integrity. (Top Left) Nanotube is secured onto AFM tip. (Center Left) Nanotube positioned over MEMS structure, then stretched across open gap (Lower Left).

Figure 10.

SEM/nanoManipulator AFM manipulation of carbon nanotube (CNT) into gap in MEMS stress/strain stage. Here the stage is used as a grabber. The tube is maneuvered into the gap (top left, center), the gap is closed (top right), pinching the CNT. The nanotube is

then stretched (lower left) while measuring electron transport until severing occurs (lower center). Lower right shows I-V curves taken before (triangles) and during stretching (open squares). After severing, the I-V showed an open circuit (diamonds).

Figure 11.

Adenovirus manipulated in ambient conditions show lateral force signatures consistent with strong initial binding and subsequent low release force for continued translation. One virus particle is selected and manipulated twice. The top right lateral force trace shows the large release peak at 300 nm where the AFM tip first contacts the virus. The second push of the same virus particle (lower right) shows a significantly lower translation force when the virus is contacted.

Figure 12.

Evidence for rolling of a virus particle upon translation is reveled through the autocorrelation of the lateral force trace after the initial release of the virus from the surface. The 23.5 nm periodicity indicated in the correlation function corresponds to a pealing of the virus at each facet of the 75 nm high icosahedral capsid.